Speed of sound and liquid-gas phase transition in nuclear matter

Wei-bo He,[1,2] Guo-yun Shao ⬥,[1,*] and Chong-long Xie[1]

[1]*MOE Key Laboratory for Non-equilibrium Synthesis and Modulation of Condensed Matter, School of Physics,*
Xi'an Jiaotong University, Xi'an 710049, China
[2]*School of Physics, Peking University, Beijing 100871, China*

We investigate the speed of sound in nuclear matter at finite temperature and density (chemical potential) in the nonlinear Walecka model. The numerical results suggest that the behaviors of sound speed are closely related to the the nuclear liquid-gas (LG) phase transition and the associated spinodal structure. The adiabatic sound speed is nonzero at the critical endpoint (CEP) in the mean-field approximation. We further derive the boundary of vanishing sound velocity in the temperature-density phase diagram, and point out the region where the sound wave equation is broken. The distinction between the speed of sound in nuclear matter and that in quark matter contains important information about the equation of state of strongly interacting matter at intermediate and high density. We also formulate the relations between differently defined speeds of sound using the fundamental thermodynamic relations.

I. INTRODUCTION

Exploring the equation of state (EOS) of strongly interacting matter is an important topic in both theoretical and experimental nuclear physics [1–25]. During the space-time evolution of the newly formed matter in heavy-ion collisions, the speed of sound is one of the crucial physical quantities to describe the variation of EOS. The dependence of speed of sound on environment (temperature, density, chemical potential, etc.) carries important information for describing the evolution of the fireball and final observables. Recently, the studies in [26–28] show that the speed of sound as a function of charged particle multiplicity $\langle dN_{ch}/d\eta \rangle$ can be extracted from heavy-ion collision data. In [29] the authors try to build a connection between the sound velocity and the baryon number cumulants to study the quantum chromodynamics (QCD) phase structure.

It is also an interesting topic to study the speed of sound during the QCD phase transition in the early universe by observing the induced gravitational wave. Although the propagation of gravitational wave is not sensitive to sound velocity, the value of sound velocity affects the dynamics of primordial density perturbations, and the induced gravitational waves by their horizon reentry can then be an indirect probe on both the EOS and sound velocity, which can provide useful knowledge of the evolution in the era of QCD phase transition [30].

Besides heavy-ion collision experiments and the early universe, the speed of sound in neutron star matter also receives a lot of attention (e.g., [31–33]). The density dependent behavior of sound velocity influences the mass-radius relation, the tidal deformability, and provides a sensitive probe of the EOS

of neutron star matter and the hadron-quark phase transition in the dense core. To obtain a massive neutron star, some studies show that it is essential for neutron star matter to have a density range where the EOS is very stiff and the corresponding squared speed of sound is significantly larger than 1/3 [31,32,34–44]. In addition, the study in [45] indicates that the speed of sound is crucial for the gravitational wave frequencies induced by the *g*-mode oscillation of a neutron star.

As an important quantity in describing the evolution of strongly interacting matter, the speed of sound in QCD matter has been calculated, e.g., in lattice QCD (LQCD) [3,46–49], the (Polyakov–)Nambu–Jona-Lasinio [(P)NJL] model [24,50–53], the quark-meson coupling model [9,54], the hadron resonance gas (HRG) model [55,56], the field correlator method (FCM) [57,58], and the quasiparticle model [59]. In most studies, the main focus is put on the region of high temperature and vanishing or small chemical potential.

In Ref. [60], we describe an intensive study on the speed of sound of QCD matter in the full phase diagram. The numerical results suggest that the dependence of sound speed on temperature, density, and chemical potential are closely related to the QCD phase structure. In particular, the value of adiabatic sound speed is not zero at the critical endpoint (CEP) in the mean-field approximation. In the region of chiral crossover, the speed of sound increases quickly with rising temperature. The value of squared sound speed approaches 1/3 after the chiral restoration at high temperature. Some new features of speed of sound are also discovered, for example the hierarchy phenomenon of sound velocity for $u(d)$ and s quarks at low temperature with the increasing chemical potential. In addition to the adiabatic sound velocity, the behaviors of speed of sound under other conditions are also discussed.

The nuclear liquid-gas (LG) phase transition was discovered in experiments many years ago, and the experimental

phenomenon was explained with the spinodal decomposition mechanism [61–69]. Recently, there were some interesting investigations on baryon number fluctuations induced by the presence of the nuclear LG phase transition [70,71]. Since the nuclear LG transition and quark chiral first-order phase transition belong to the same universality class, it is interesting to study whether the speeds of sound in quark matter and in nuclear matter behave in a similar way. Moreover, the study on the parameter dependence of the speed of sound in nuclear matter is crucial for investigating the transport phenomenon of hadronic matter [24]. In this study, we will explore in detail the behavior of sound speed in nuclear matter and compare it with that in quark matter. It is expected that the correlation between the behaviors of speed of sound and nuclear LG phase transition can be revealed.

The paper is organized as follows. In Sec. II, we introduce briefly the nonlinear Walecka model and the formulas of speed of sound under different definitions. In Sec. III, we present the numerical results of squared sound speed and discuss the relations with the nuclear LG transition. A summary is given in Sec. IV.

II. THE NONLINEAR WALECKA MODEL AND SPEED OF SOUND

The Lagrangian density for the nucleons-meson system in the nonlinear Walecka model [72] is

$$
\begin{aligned}
\mathcal{L} = \sum_N \bar{\psi}_N [i\gamma_\mu \partial^\mu - (m_N - g_\sigma \sigma) - g_\omega \gamma_\mu \omega^\mu]\psi_N \\
+ \frac{1}{2}(\partial_\mu \sigma \partial^\mu \sigma - m_\sigma^2 \sigma^2) - \frac{1}{3}bm_N(g_\sigma \sigma)^3 - \frac{1}{4}c(g_\sigma \sigma)^4 \\
+ \frac{1}{2}m_\omega^2 \omega_\mu \omega^\mu - \frac{1}{4}\omega_{\mu\nu}\omega^{\mu\nu},
\end{aligned}
\tag{1}
$$

where $\omega_{\mu\nu} = \partial_\mu \omega_\nu - \partial_\nu \omega_\mu$. The interactions between nucleons are mediated by σ, ω mesons. The ρ meson is not included since in this work we only consider the behavior of speed of sound in symmetric nuclear matter. The model parameters, g_σ, g_ω, b, and c are fixed in the mean-field approximation with the compression modulus $K = 240$ MeV, the symmetric energy $a_{sym} = 31.3$ MeV, the effective nucleon mass $m_N^* = m_N - g_\sigma \sigma = 0.75 m_N$ (m_N is the nucleon mass in vacuum), and the binding energy $B/A = -16.0$ MeV at nuclear saturation density with $\rho_0 = 0.16$ fm^{-3}.

The thermodynamic potential derived under the mean-field approximation is

$$
\begin{aligned}
\Omega = -\beta^{-1} \sum_N 2 \int \frac{d^3 k}{(2\pi)^3} [\ln(1 + e^{-\beta[E_N^*(k) - \mu_N^*]}) \\
+ \ln(1 + e^{-\beta[E_N^*(k) + \mu_N^*]})] + \frac{1}{2}m_\sigma^2 \sigma^2 + \frac{1}{3}bm_N(g_\sigma \sigma)^3 \\
+ \frac{1}{4}c(g_\sigma \sigma)^4 - \frac{1}{2}m_\omega^2 \omega^2,
\end{aligned}
\tag{2}
$$

where $\beta = 1/T$, $E_N^* = \sqrt{k^2 + m_N^{*2}}$. The effective chemical potential μ_N^* is defined as $\mu_N^* = \mu_N - g_\omega \omega$ for nucleons.

By minimizing the thermodynamical potential

$$
\frac{\partial \Omega}{\partial \sigma} = \frac{\partial \Omega}{\partial \omega} = 0,
\tag{3}
$$

the meson field equations are derived as

$$
g_\sigma \sigma = \left(\frac{g_\sigma}{m_\sigma}\right)^2 [\rho_p^s + \rho_n^s - bm_N(g_\sigma \sigma)^2 - c(g_\sigma \sigma)^3],
\tag{4}
$$

$$
g_\omega \omega = \left(\frac{g_\omega}{m_\omega}\right)^2 (\rho_p + \rho_n).
\tag{5}
$$

In Eqs. (4) and (5), the nucleon number density for proton or neutron is

$$
\rho_N = 2 \int \frac{d^3 \boldsymbol{k}}{(2\pi)^3}[f(E_N^*(k) - \mu_N^*) - \bar{f}(E_N^*(k) + \mu_N^*)],
\tag{6}
$$

and the scalar density

$$
\rho_N^s = 2 \int \frac{d^3 \boldsymbol{k}}{(2\pi)^3} \frac{m_N^*}{E_N^*(k)}[f(E_N^*(k) - \mu_N^*) + \bar{f}(E_N^*(k) + \mu_N^*)],
\tag{7}
$$

where $f(E_N^*(k) - \mu_N^*)$ and $\bar{f}(E_N^*(k) + \mu_N^*)$ are the fermion and antifermion distribution functions.

The pressure p and energy density ϵ can be derived using the thermodynamic relations in the grand canonical ensemble as

$$
p = -\Omega, \quad \epsilon = -p + Ts + \sum \mu_N \rho_N,
\tag{8}
$$

where s is the entropy density. The general definition of speed of sound is

$$
c_X^2 = \left(\frac{\partial p}{\partial \epsilon}\right)_X.
\tag{9}
$$

A specific constant quantity X is required to describe the propagation of the compression wave through a medium. To indicate the different profiles of the EOS of nuclear matter, X can be chosen as s/ρ_B, s, ρ_B, T, μ_B.

For an ideal fluid, it evolves with a constant entropy density per baryon, s/ρ_B, under the adiabatic evolution. This conclusion can be drawn in hydrodynamics with the conservation of energy and baryon number, therefore it is most meaningful to calculate the speed of sound along the isentropic curve

$$
c_{s/\rho_B}^2 = \left(\frac{\partial p}{\partial \epsilon}\right)_{s/\rho_B}.
\tag{10}
$$

The dependence of c_{s/ρ_B}^2 on parameters, e.g., temperature, density, and chemical potential, can indicate the variation of sound speed during the evolution and provide important knowledge of interaction, phase transition, and the EOS.

The definitions of sound velocity under other conditions are also taken in literature in dealing with different problems. The speed of sound with constant baryon number density or entropy density are taken in describing the intermediate

process of hydrodynamic evolution [24,73],

$$c_{\rho_B}^2 = \left(\frac{\partial p}{\partial \epsilon}\right)_{\rho_B} \qquad (11)$$

and

$$c_s^2 = \left(\frac{\partial p}{\partial \epsilon}\right)_s . \qquad (12)$$

For example, the space-time derivatives of temperature and chemical potential are functions of $c_{\rho_B}^2$ and c_s^2 with

$$\partial_0 \mu_B = -c_s^2 \mu_B \nabla \cdot \mathbf{u} \qquad (13)$$

and

$$\partial_0 T = -c_{\rho_B}^2 T \nabla \cdot \mathbf{u}, \qquad (14)$$

where $\mathbf{u}$ denotes the space component of four-velocity.

It is also interesting to calculate the sound velocity with a fixed temperature or chemical potential with

$$c_T^2 = \left(\frac{\partial p}{\partial \epsilon}\right)_T \qquad (15)$$

and

$$c_{\mu_B}^2 = \left(\frac{\partial p}{\partial \epsilon}\right)_{\mu_B} . \qquad (16)$$

c_T^2 is widely used in calculating the sound speed in neutron star matter. In [29] the authors make a connection between the logarithmic derivative of c_T^2 with respect to baryon density and baryon number fluctuations, which can be measured in experiment.

In this study, we will explore the speed of sound in nuclear matter under different definitions in the full temperature-density and temperature-chemical potential spaces. Since the general definitions given above can only be used to calculate the speed of sound along special trajectories, it is necessary to derive the corresponding formulas as functions of T and μ_B (ρ_B) to perform the calculation for any given temperature and density (chemical potential).

Using the fundamental thermodynamic relations, we derive the sound speed formulas under different conditions in terms of T and μ_B as

$$c_{s/\rho_B}^2 = \frac{s\rho_B\left(\frac{\partial s}{\partial \mu_B}\right)_T - s^2\left(\frac{\partial \rho_B}{\partial \mu_B}\right)_T - \rho_B^2\left(\frac{\partial s}{\partial T}\right)_{\mu_B} + s\rho_B\left(\frac{\partial \rho_B}{\partial T}\right)_{\mu_B}}{(sT + \mu_B\rho_B)\left[\left(\frac{\partial s}{\partial \mu_B}\right)_T\left(\frac{\partial \rho_B}{\partial T}\right)_{\mu_B} - \left(\frac{\partial s}{\partial T}\right)_{\mu_B}\left(\frac{\partial \rho_B}{\partial \mu_B}\right)_T\right]}, \qquad (17)$$

$$c_{\rho_B}^2 = \frac{s\left(\frac{\partial \rho_B}{\partial \mu_B}\right)_T - \rho_B\left(\frac{\partial \rho_B}{\partial T}\right)_{\mu_B}}{T\left[\left(\frac{\partial s}{\partial T}\right)_{\mu_B}\left(\frac{\partial \rho_B}{\partial \mu_B}\right)_T - \left(\frac{\partial s}{\partial \mu_B}\right)_T\left(\frac{\partial \rho_B}{\partial T}\right)_{\mu_B}\right]}, \qquad (18)$$

$$c_s^2 = \frac{s\left(\frac{\partial s}{\partial \mu_B}\right)_T - \rho_B\left(\frac{\partial s}{\partial T}\right)_{\mu_B}}{\mu_B\left[\left(\frac{\partial \rho_B}{\partial T}\right)_{\mu_B}\left(\frac{\partial s}{\partial \mu_B}\right)_T - \left(\frac{\partial s}{\partial T}\right)_{\mu_B}\left(\frac{\partial \rho_B}{\partial \mu_B}\right)_T\right]}, \qquad (19)$$

$$c_T^2 = \frac{\rho_B}{T\left(\frac{\partial s}{\partial \mu_B}\right)_T + \mu_B\left(\frac{\partial \rho_B}{\partial \mu_B}\right)_T}, \qquad (20)$$

$$c_{\mu_B}^2 = \frac{s}{T\left(\frac{\partial s}{\partial T}\right)_{\mu_B} + \mu_B\left(\frac{\partial \rho_B}{\partial T}\right)_{\mu_B}}. \qquad (21)$$

The corresponding sound speed formulas derived in terms of T and ρ_B are

$$c_{s/\rho_B}^2 = \frac{s^2 + \rho_B^2\left[\left(\frac{\partial \mu_B}{\partial \rho_B}\right)_T\left(\frac{\partial s}{\partial T}\right)_{\rho_B} - \left(\frac{\partial \mu_B}{\partial T}\right)_{\rho_B}\left(\frac{\partial s}{\partial \rho_B}\right)_T\right] + s\rho_B\left[\left(\frac{\partial \mu_B}{\partial T}\right)_{\rho_B} - \left(\frac{\partial s}{\partial \rho_B}\right)_T\right]}{(Ts + \mu_B\rho_B)\left(\frac{\partial s}{\partial T}\right)_{\rho_B}}, \qquad (22)$$

$$c_{\rho_B}^2 = \frac{s + \rho_B\left(\frac{\partial \mu_B}{\partial T}\right)_{\rho_B}}{T\left(\frac{\partial s}{\partial T}\right)_{\rho_B}}, \qquad (23)$$

$$c_s^2 = \frac{\rho_B\left[\left(\frac{\partial s}{\partial T}\right)_{\rho_B}\left(\frac{\partial \mu_B}{\partial \rho_B}\right)_T - \left(\frac{\partial s}{\partial \rho_B}\right)_T\left(\frac{\partial \mu_B}{\partial T}\right)_{\rho_B}\right] - s\left(\frac{\partial s}{\partial \rho_B}\right)_T}{\mu_B\left(\frac{\partial s}{\partial T}\right)_{\rho_B}}, \qquad (24)$$

$$c_T^2 = \frac{\rho_B\left(\frac{\partial \mu_B}{\partial \rho_B}\right)_T}{T\left(\frac{\partial s}{\partial \rho_B}\right)_T + \mu_B}, \qquad (25)$$

$$c_{\mu_B}^2 = \frac{s\left(\frac{\partial \mu_B}{\partial \rho_B}\right)_T}{T\left[\left(\frac{\partial s}{\partial T}\right)_{\rho_B}\left(\frac{\partial \mu_B}{\partial \rho_B}\right)_T - \left(\frac{\partial \mu_B}{\partial T}\right)_{\rho_B}\left(\frac{\partial s}{\partial \rho_B}\right)_T\right] - \mu_B\left(\frac{\partial \mu_B}{\partial T}\right)_{\rho_B}}. \qquad (26)$$

III. NUMERICAL RESULTS AND DISCUSSIONS

In this section, we present the phase structure of symmetric nuclear matter and the numerical results of the speed of sound under different definitions at finite temperature and baryon density (chemical potential), and discuss the relations between the speed of sound and nuclear LG phase transition. Symmetric nuclear matter is considered in this study to describe the essential behavior of speed of sound.
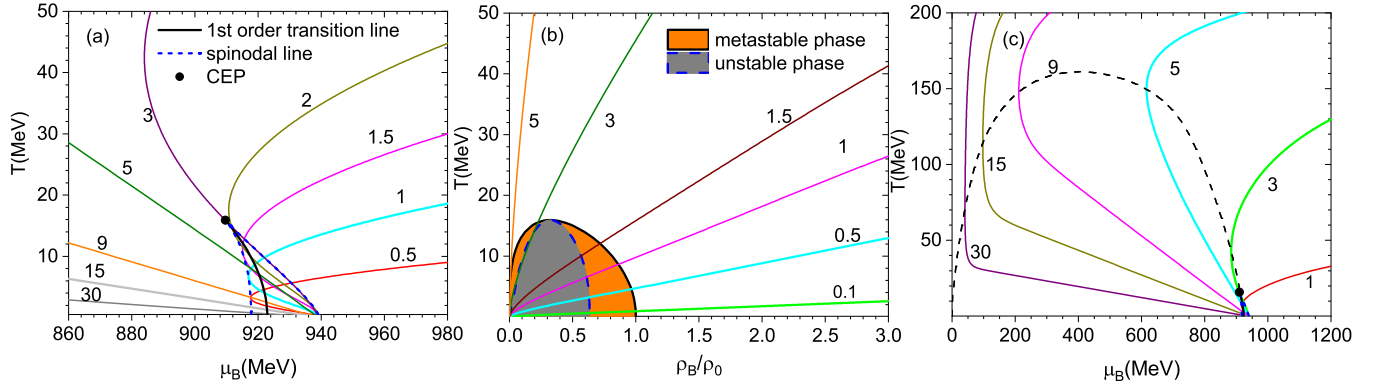
FIG. 1. Phase diagram of nuclear liquid-gas transition and the isentropic curves for different values of s/ρ_B. (a) Spinodal structure of LG phase transition the in T-μ_B plane. (b) Phase structure of LG phase transition in T-ρ_B plane. (c) Isentropic trajectories in the T-μ_B phase diagram; the black dashed line is derived with $(\frac{\partial \mu_B}{\partial T})_{s/\rho_B} = 0$.

A. Nuclear liquid-gas phase transition and speed of sound at constant s/ρ_B

First, we demonstrate in Fig. 1 the phase structure of nuclear LG phase transition and the isentropic curves for different values of s/ρ_B. Figures 1(a) and 1(b) show the details of nuclear LG phase transition and the corresponding spinodal structure. The black solid line is the first-order phase transition line, and the blue dashed line is the boundary of spinodal structure associated with the nuclear LG phase transition. Fiure 1(b) shows clearly that the two curves separate the phase diagram into the stable, metastable, and unstable phases. The spinodal phase decomposition plays a dominant role in the experimental exploration of the first-order nuclear LG tran-sition [67,71]. It has also inspired the anticipation to identify the first-order chiral phase transition in high-energy heavy-ion collisions through the spinodal phase separation [74–83].

The first-order transition line and the spinodal line meet at the CEP. The isentropic curves in Fig. 1 indicate the evolution-ary trajectories of an ideal fluid under the adiabatic condition. Figure 1(b) shows that for smaller s/ρ_B the evolutionary tra-jectories pass through the stable, metastable, and unstable phases. It is expected that important information on the phase transition is carried by the speed of sound. Figiure 1(c) shows the nuclear LG transition and isentropic trajectories in the full $T - \mu_B$ phase diagram. In Fig. 1(c), we also plot the boundary of $(\frac{\partial \mu_B}{\partial T})_{s/\rho_B} = 0$ (black dashed curve), which is closely related to the behavior of sound speed at constant entropy density.

We present the squared speed of sound c^2_{s/ρ_B} as functions of baryon chemical potential for different temperatures in Fig. 2 and the contour map in Fig. 3. Figure 2 shows that c^2_{s/ρ_B} grows with the increase of chemical potential for each temperature. It also indicates that, for $\mu_B < 1320$ MeV, c^2_{s/ρ_B} at a higher tem-perature is larger than that at a lower temperature, because the pressure and energy density is mainly driven by temperature for small chemical potential. For $\mu_B > 1320$ MeV, the oppo-site happens, which is mainly attributed to the density-driven effect with the decrease of dynamic mass of the nucleon. For $T = 10$ MeV, a small jump of c^2_{s/ρ_B} appears on the boundary of the first-order phase transition.

The contour map in Fig. 3 demonstrates the profiles of c^2_{s/ρ_B} in the full T-μ_B phase diagram with the nuclear LG phase transition. In this figure we also plot the fitted chemical freeze-out line. The parametrized formula of the freeze-out line is taken from Ref. [20] with

$$\mu_B(\sqrt{s_{NN}}) = \frac{1.477}{1 + 0.343\sqrt{s_{NN}}} \qquad (27)$$

and

$$T(\mu_B) = a - b\mu_B^2 - c\mu_B^4, \qquad (28)$$

where $a = 0.158$ GeV, $b = 0.14$ GeV^{-1}, and c varies from 0.04 to 0.12. The chemical freeze-out curve in Fig. 3 is plotted for the intermediate value of $c = 0.08$. The value of c^2_{s/ρ_B} along the freeze-out line is given in Fig. 4. It shows that c^2_{s/ρ_B} on the freeze-out line changes slightly for collision energy larger than 10 GeV. A small peak appears at $\sqrt{s_{NN}} \simeq 6$ GeV, and c^2_{s/ρ_B} decreases with the decline of collision energy.
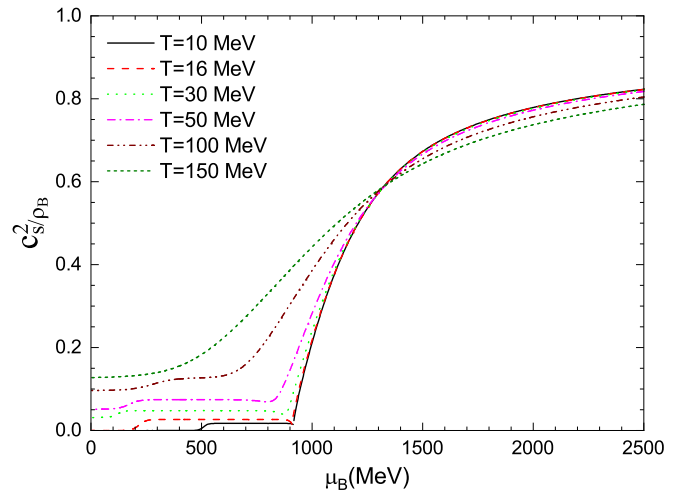

FIG. 2. Squared sound speed c^2_{s/ρ_B} as functions of chemical po-tential for several fixed temperatures.
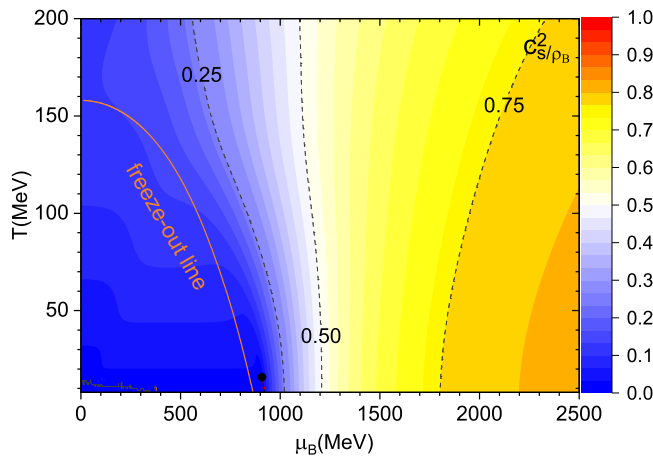
FIG. 3. Contour map of c_{s/ρ_B}^2 in the T-μ_B plane.

FIG. 5. Values of c_{s/ρ_B}^2 on the boundary of first-order transition and the "crossover" line.

We can also see that the chemical freeze-out line at low temperature is close to the nuclear LG phase transition. We display the value of c_{s/ρ_B}^2 on the boundary of the nuclear LG phase transition in Fig. 5. The blue solid line is the value along the low-density side of the first-order phase transition and the black solid line is the result on the high-density side. The dash-dotted line is the "crossover" line, which is derived with $\partial\sigma/\partial\mu_B$ (or $\partial m_N^*/\partial\mu_B$) taking the extremum for a given temperature. This is inspired by the description of quark chiral phase transition in quark models. The aim of plotting the "crossover" line is to show that some thermodynamic properties are sensitive to this line. Such a description is also used to discuss the net baryon number fluctuations induced by the nuclear LG phase transition [71].

Figure 5 indicates that the square of sound speed is not zero but a small value at the CEP. It is a feature of the mean-field approximation. A similar behavior exists for the quark chiral phase transition in the PNJL model with the mean-field assumption [60]. Figure 5 also suggests that the value of c_{s/ρ_B}^2 is small near the first-order transition region. Since only the
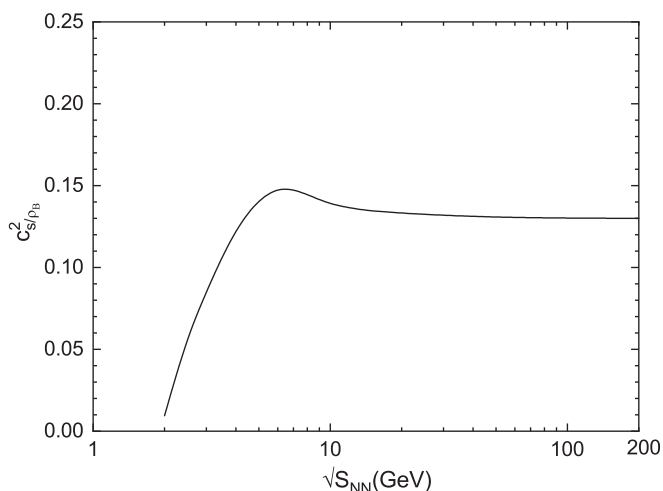
stable phase is considered in the above discussion, it cannot give a complete demonstration of sound speed along the isentropic trajectories. Therefore, we further present in Fig. 6 the contour map of c_{s/ρ_B}^2 in the full T-ρ_B plane, including all the stable, metastable, and unstable phases.

In Fig. 6, besides the first-order phase transition line (black solid line) and the spinodal line (red dashed line), we also derive the boundary of vanishing sound speed, which is plotted with the yellow dashed line. At each point of this boundary, it fulfills the condition of $(\frac{\partial p}{\partial \epsilon})_{s/\rho_B} = 0$. Inside this boundary (grey area), the value of $c_{s/\rho_B}^2 = (\frac{\partial p}{\partial \epsilon})_{s/\rho_B}$ is negative. The sound wave equation is broken in this situation, and becomes a decay function. It means that a disturbance cannot be propagated in this region.

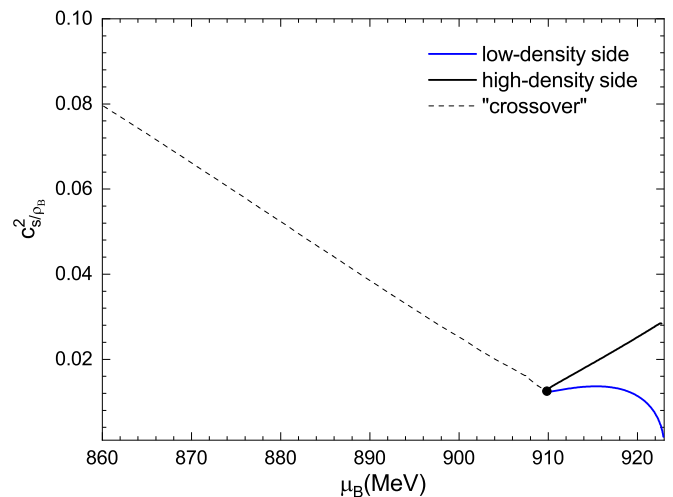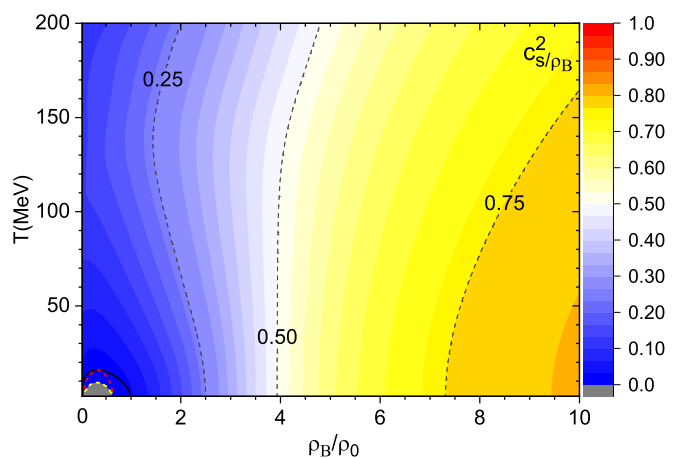FIG. 4. Values of c_{s/ρ_B}^2 along the chemical freeze-out line as a function of collision energy.

FIG. 6. Contour map of c_{s/ρ_B}^2 in the T-ρ_B plane. The black solid line is the first-order phase transition line. The red dashed line is the spinodal line. The yellow dashed line is the boundary of vanishing sound speed. Both the red dashed line and the yellow dashed line are located near the origin of the coordinate system (bottom left of the figure).
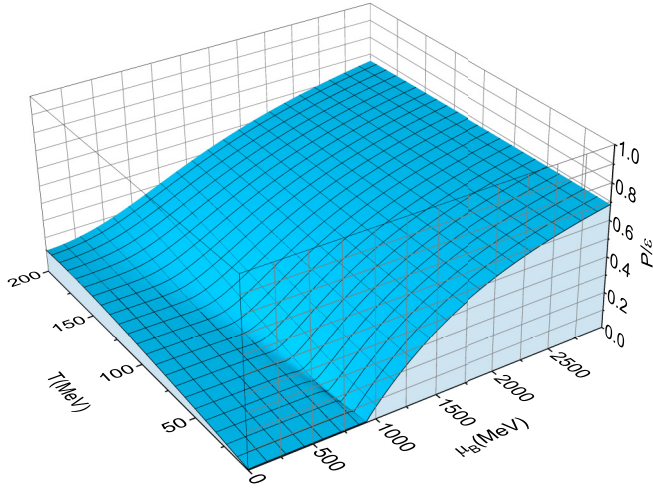
FIG. 7. 3D map of p/ϵ as a function of temperature and chemical potential.

FIG. 9. Contour map of $c_{\rho_B}^2$ in the T-ρ_B plane. The black solid line is the first-order phase transition line. The red dashed line is the spinodal line located near the origin of the coordinate system (bottom left of the figure).

From Figs. 2, 3, and 6, we can see that the square of sound speed is quite larger than $1/3$ at high density (large chemical potential), about 0.8 being approached at very large chemical potential. However, the value of c_{s/ρ_B}^2 in quark matter approaches $1/3$ at high density [60]. To understand the variation of speed of sound in nuclear matter, we plot the three-dimensional (3D) map of p/ϵ as a function of the temperature and chemical potential in Fig. 7. It indicates that the behavior of p/ϵ is responsible for the growing speed of sound from low to high chemical potential.

The interaction measurement or trace anomaly is defined as $\epsilon - 3p$, which can effectively describe the interaction in a thermal system. We demonstrate the value of $(\epsilon - 3p)/\epsilon$ of symmetric nuclear matter in Fig. 8. Comparing it with the phase transition line, we find that the behavior of $(\epsilon - 3p)/\epsilon$ is related to the nuclear phase transition. The behavior of

$(\epsilon - 3p)/\epsilon$ reflects the variation of nucleon mass or the σ meson field, i.e., the interaction between nucleons. Moreover, we can see that $(\epsilon - 3p)/\epsilon$ in nuclear matter does not approach zero at large chemical potential, quietly different from that of quark matter.

The calculation in the Walecka model and PNJL model indicate that the speed of sound in nuclear matter is quite larger than that in quark matter at high density. Theoretically, in the Walecka model, the ω meson interaction is proportional to the baryon density, leading to a steady increase in the speed of sound, with the limiting value of 1 at $\rho_B \to \infty$. In the (P)NJL model, the value of the sigma mean field, and therefore of the corresponding interaction, decreases with density. In view of this the (P)NJL model looks like a gas of noninteracting relativistic particles at $\rho_B \to \infty$. To the extent that the Walecka model can be thought to describe nuclear matter and the (P)NJL model can give one some insight of high-density quark matter. If a phase transition from nuclear matter to quark matter takes place with growing density, the
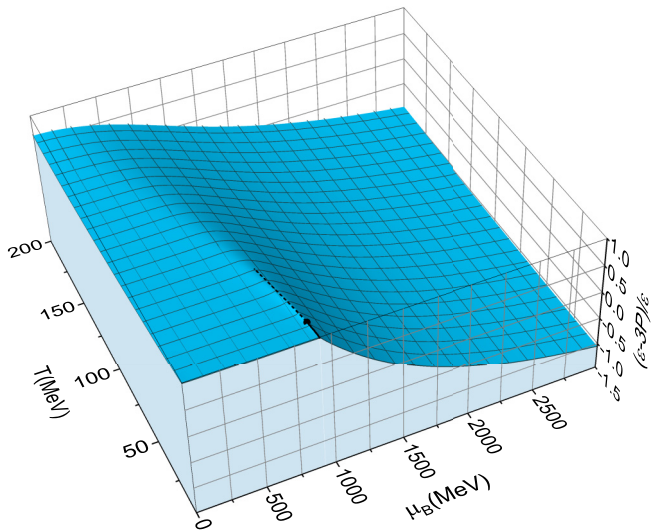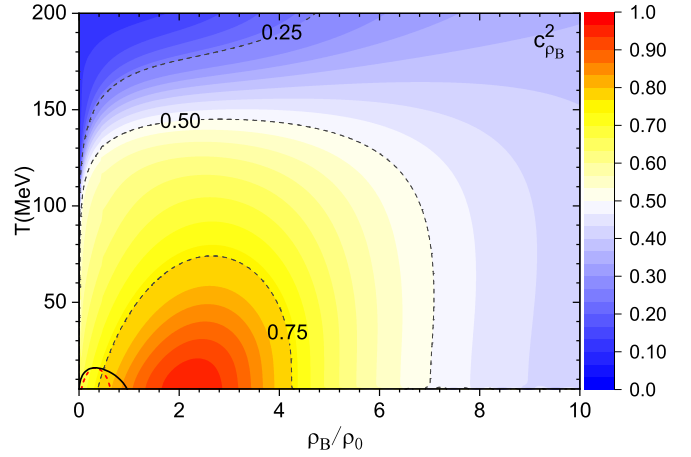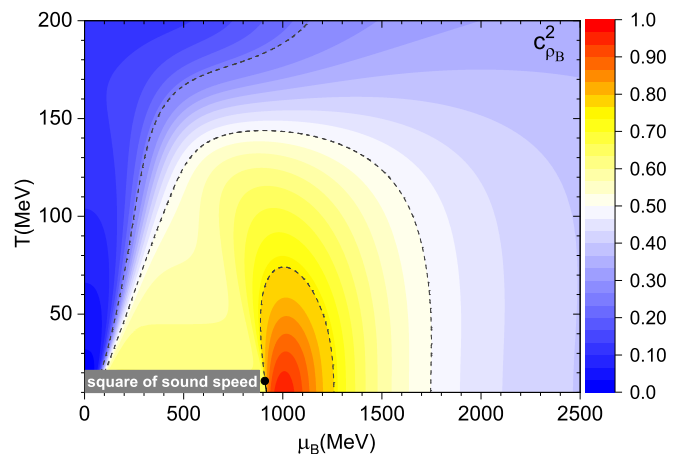

FIG. 8. 3D map of $(\epsilon - 3p)/\epsilon$ as a function of temperature and chemical potential. The black solid line is the nuclear LG phase transition line. The black dashed line is the "crossover" line [71].

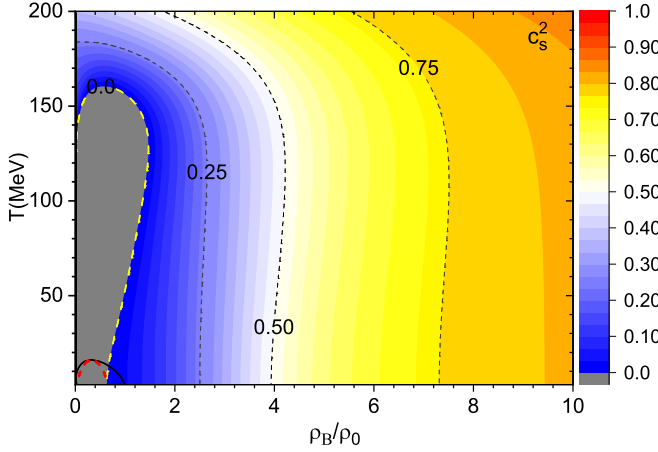FIG. 10. Contour map of $c_{\rho_B}^2$ in the T-μ_B plane.

FIG. 11. Contour map of c_s^2 in the T-ρ_B plane. The black solid line is the first-order phase transition line. The red dashed line is the spinodal line located near the origin of the coordinate system (bottom left of the figure). The yellow dashed line marked with 0.0 is the boundary where the value of c_s^2 vanishes. $c_s^2 = (\partial p/\partial \epsilon)_s$ is negative inside the yellow dashed line.

value of speed of sound will have a peak at a certain density. It is interesting that recent neutron star research suggests that the value of the speed of sound first increases sharply with ρ_B, exceeding the conformal value of $1/3$, then falls again below $1/3$, and finally approaches $1/3$ at infinity from below. It is anticipated to give a further analysis on the speed of sound of neutron star matter with different phase transition mechanism and observation constraints.

B. Speed of sound at constant ρ_B or s

We plot the contour map of the squared speed of sound $c_{\rho_B}^2$ in the T-ρ_B plane in Fig. 9 and the T-μ_B plane in Fig. 10. The numerical results indicate that the value of $c_{\rho_B}^2$ lies in the range of 0–1. For most temperatures, $c_{\rho_B}^2$ shows a nonmonotonic behavior with the increase of density or chemical potential. In particular, a peaklike structure exists at intermediate density (chemical potential).

We present the squared speed of sound c_s^2 at constant entropy density in Figs. 11 and 12. The two figures indicate that the contour of c_s^2 has a relatively complicated structure. The value of c_s^2 are divided into two parts by the yellow dashed curve. Outside the curve, the value of c_s^2 is positive and smaller than 1. Inside the curve (gray area), c_s^2 is negative. The value of c_s^2 vanishes on the boundary given by the yellow dashed curve. Such a feature is possibly general for a first-order phase transition in a interacting system with temperature and density dependent fermion mass, and a similar structure for the speed of sound in quark matter is found in Ref. [60].

In fact, the boundary (yellow dashed line) in Figs. 11 and 12 is just the curve shown in Fig. 1(c). This can be proved with the thermodynamics formula

$$\left(\frac{\partial \mu_B}{\partial T}\right)_{s/\rho_B} = \frac{\mu_B}{T}\frac{\left(\frac{\partial p}{\partial \epsilon}\right)_s}{\left(\frac{\partial p}{\partial \epsilon}\right)_{\rho_B}} = \frac{\mu_B}{T}\frac{c_s^2}{c_{\rho_B}^2}. \tag{29}$$
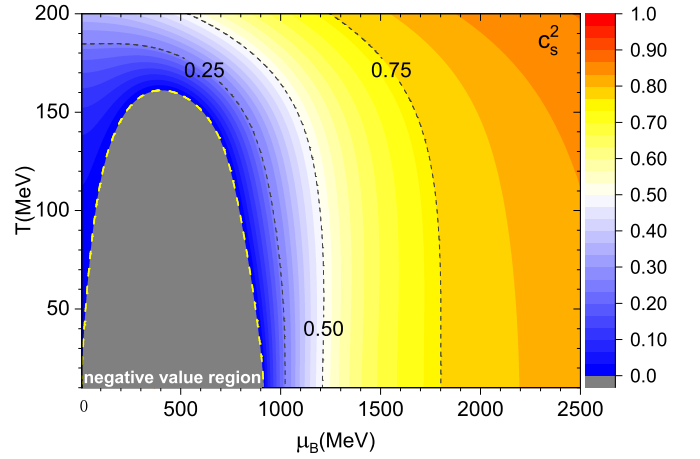

FIG. 12. Contour map of c_s^2 in the T-μ_B plane. The yellow dashed line is the boundary where the value of c_s^2 vanishes. $c_s^2 = (\partial p/\partial \epsilon)_s$ is negative inside the yellow dashed line.

Using Eqs. (29) we can obtain the boundary of vanishing c_s^2 by taking $(\frac{\partial \mu_B}{\partial T})_{s/\rho_B} = 0$. This is the physical condition used to derive the dashed curve in Fig. 1(c). Moreover, when the condition $(\frac{\partial \mu_B}{\partial T})_{s/\rho_B} < 0$ is fulfilled, one of the two physical quantities c_s^2 and $c_{\rho_B}^2$ takes a negative value. There indeed exists such a region in the phase diagram, as shown in Fig. 1(c) (inside the black dashed curve). Since $c_{\rho_B}^2$ is always positive, $c_s^2 = (\partial p/\partial \epsilon)_s$ is negative in this situation. The blue areas in Figs. 11 and 12 indicate the negative region.

Comparing the result with that of quark matter in the PNJL model (Fig. 1 in Ref. [60]), we find there are three regions in which $(\frac{\partial \mu_B}{\partial T})_{s/\rho_B} < 0$ for quark matter, including the lower left of the T-μ_B phase diagram and a small neighboring area of chiral-crossover transformation near the CEP, as well as a part of the region where the chiral symmetry of u, d quarks is restored but the Polyakov loop is still confining. Correspondingly, c_s^2 or $c_{\rho_B}^2$ is negative in the these regions. One can refer to Ref. [60] for details.

C. Speed of sound at constant T or μ_B

In the following, we study the speed of sound derived at constant T or μ_B. Recently, the density dependent c_T^2 has been discussed for neutron star matter under the equilibrium of weak interaction. The data from observations support a large value of c_T^2 (larger than $1/3$) at a few times nuclear saturation density. In [29] the authors also try to estimate c_T^2 at chemical freeze-out of quark-gluon plasma using the baryon number fluctuations of the beam energy scan experiments at the BNL Relativistic Heavy Ion Collider (RHIC). We explore here the behavior of c_T^2 and $c_{\mu_B}^2$ in nuclear matter in the full T-ρ_B and T-μ_B phase diagram.

Figures 13 and 14 demonstrate the contour maps of c_T^2 in the T-ρ_B and T-μ_B planes, respectively. The two figures show that the value of c_T^2 increases with the rising density or chemical potential in the stable phase, and causality is always satisfied with $c_T^2 < 1$. The value of c_T^2 is close to c_{s/ρ_B}^2 at low temperature, since the isentropic trajectories are
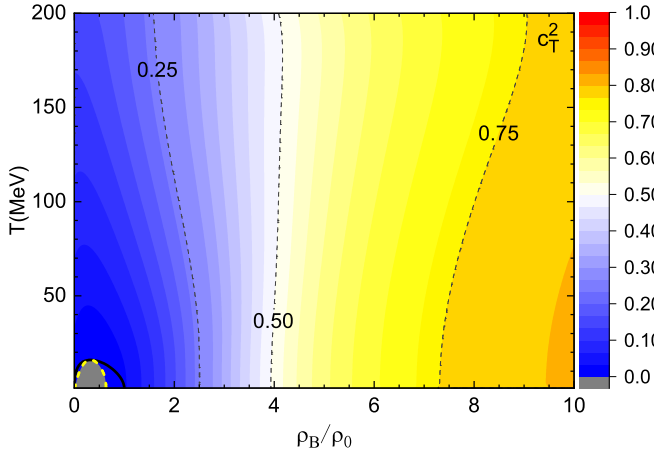
FIG. 13. Contour map of c_T^2 in the T-ρ_B plane. The yellow dashed curve located near the origin of the coordinate system (bottom left of the figure) is the spinodal line and the boundary of $c_T^2 = 0$. $c_T^2 = (\partial p/\partial \epsilon)_T$ is negative inside the boundary.

FIG. 15. Contour map of $c_{\mu_B}^2$ in the T-ρ_B plane. The yellow dashed curve located near the origin of the coordinate system (bottom left of the figure) is the spinodal line and the boundary of $c_{\mu_B}^2 = 0$. $c_{\mu_B}^2 = (\partial p/\partial \epsilon)_{\mu_B}$ is negative inside the boundary.

approximately parallel to the density or chemical potential axis as indicated in Fig. 1. The behavior of c_T^2 in nuclear matter at low temperature is to some extent similar to that of neutron star matter under β equilibrium. Combined with the behavior of c_T^2 in quark matter, if a hadron-quark phase transition happens at high density, the value of c_T^2 will decrease in the mixed phase or pure quark phase. A detailed study of the speed of sound in neutron star matter is in progress.

Figure 13 also demonstrates that there exists a region (gray area) where $c_T^2 = (\frac{\partial p}{\partial \epsilon})_T < 0$. This region is just the unstable phase derived with the thermodynamic stability conditions. On the boundary of spinodal line including the CEP of the first-order transition, the value of c_T^2 is zero. c_T^2 is positive in both the stable and metastable phases.

We display the contour map of $c_{\mu_B}^2$ in Figs. 15 and 16. Similarly to Fig. 13, the contour map in Fig. 15 indicates that $c_{\mu_B}^2 = (\partial p/\partial \epsilon)_{\mu_B} < 0$ inside the spinodal line. $c_{\mu_B}^2$ is positive in the metastable and stable phases. The contour maps in Figs. 15 and 16 also indicate that the value of $c_{\mu_B}^2$ has a peaklike structure in the phase diagram.
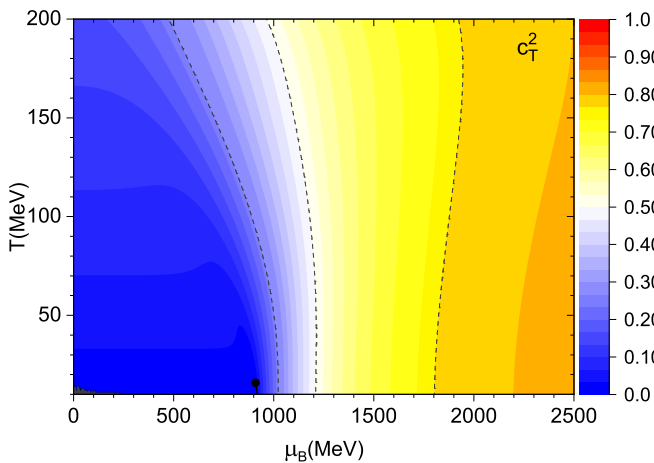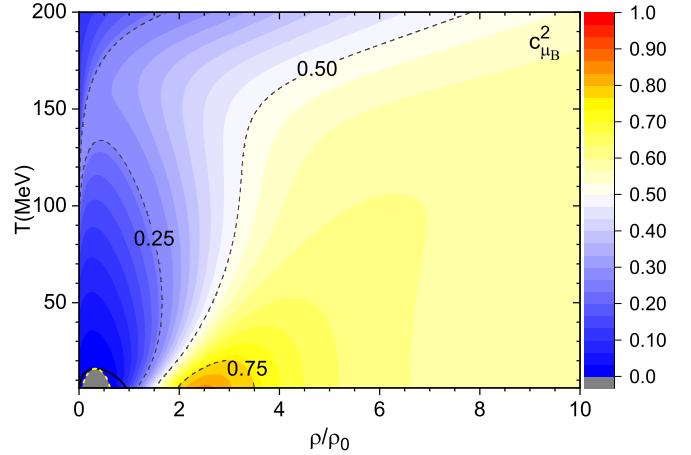
Finally, we note that the numerical results at high temperature should be treated with caution, since more hadronic degrees of freedom will appear at high temperature. In this study, we show the numerical results in the full phase diagram in order to demonstrate the whole changing trend of speed of sound.

IV. SUMMARY

In this work, we studied the speed of sound in symmetric nuclear matter at finite temperature and density (chemical potential) in the nonlinear Walecka model. We derived the speed of sound under different definitions in the complete phase diagram including the stable, metastable, and unstable phases associated with the first-order phase transition. We systematically discussed the relations between the speed of sound and nuclear LG phase transition.

The numerical results indicate that the behavior of the speed of sound in the phase diagram is closely related the phase structure of nuclear matter. From the perspective of
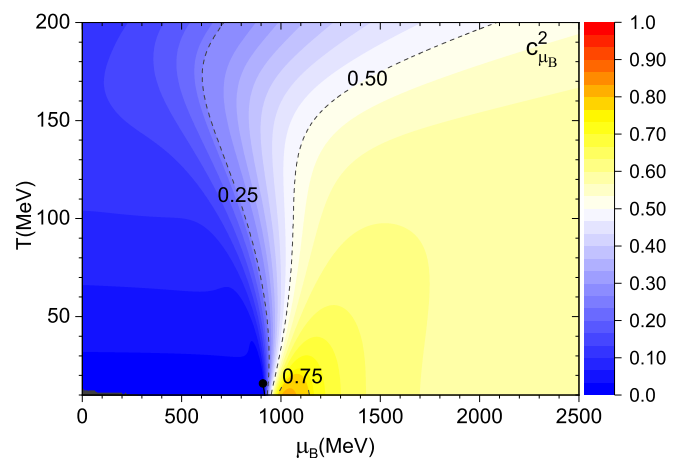

FIG. 14. Contour map of c_T^2 in the T-μ_B plane.

FIG. 16. Contour map of $c_{\mu_B}^2$ in the T-μ_B plane.

ideal fluid evolution, we focus on exploring the behavior of adiabatic sound velocity at constant s/ρ_B. The calculation indicates that the sound speed c^2_{s/ρ_B} is nonzero at the CEP under the mean-field approximation, and the boundary of vanishing sound velocity is derived. We also found that the value of c^2_{s/ρ_B} is much larger than $1/3$ at high density, different from that in quark matter where c^2_{s/ρ_B} approaches $1/3$ at high density and/or high temperature.

We also explored the behaviors of sound speed under different physical conditions, and analyzed the correlations with the nuclear LG phase transition, as well as the relations between different definitions. The calculation shows that it is natural in nuclear matter to have a sound speed larger than $\sqrt{1/3}$ at a few times nuclear saturation density. A further study on the speed of sound in neutron star matter with a hadron-quark phase transition and observation constraints will be performed in the future.

[1] S. Gupta, X. F. Luo, B. Mohanty, H. G. Ritter, and N. Xu, Science **332**, 1525 (2011).

[2] A. Bazavov, H. T. Ding, P. Hegde, O. Kaczmarek, F. Karsch, E. Laermann *et al.* (HotQCD Collaboration), Phys. Rev. D **96**, 074510 (2017).

[3] S. Borsányi, Z. Fodor, J. N. Guenther, R. Kara, S. D. Katz, P. Parotto, A. Pasztor, C. Ratti, and K. K. Szabo, Phys. Rev. Lett. **125**, 052001 (2020).

[4] K. Fukushima, Phys. Rev. D **77**, 114028 (2008).

[5] C. Ratti, M. A. Thaler, and W. Weise, Phys. Rev. D **73**, 014019 (2006).

[6] P. Costa, M. C. Ruivo, C. A. de Sousa, and H. Hansen, Symmetry **2**, 1338 (2010).

[7] T. Sasaki, J. Takahashi, Y. Sakai, H. Kouno, and M. Yahiro, Phys. Rev. D **85**, 056009 (2012).

[8] M. Ferreira, P. Costa, and C. Providência, Phys. Rev. D **89**, 036006 (2014).

[9] B. J. Schaefer, M. Wagner, and J. Wambach, Phys. Rev. D **81**, 074013 (2010).

[10] V. Skokov, B. Friman, and K. Redlich, Phys. Rev. C **83**, 054904 (2011).

[11] S. X. Qin, L. Chang, H. Chen, Y. X. Liu, and C. D. Roberts, Phys. Rev. Lett. **106**, 172301 (2011).

[12] F. Gao, J. Chen, Y. X. Liu, S. X. Qin, C. D. Roberts, and S. M. Schmidt, Phys. Rev. D **93**, 094019 (2016).

[13] C. S. Fischer, J. Luecker, and C. A. Welzbacher, Phys. Rev. D **90**, 034022 (2014).

[14] W. J. Fu, J. M. Pawlowski, and F. Rennecke, Phys. Rev. D **101**, 054032 (2020).

[15] M. A. Stephanov, Phys. Rev. Lett. **102**, 032301 (2009); **107**, 052301 (2011).

[16] G. Y. Shao, Z. D. Tang, X. Y. Gao, and W. B. He, Eur. Phys. J. C **78**, 138 (2018).

[17] G. Y. Shao, W. B. He, and X. Y. Gao, Phys. Rev. D **100**, 014020 (2019).

[18] X. Luo (STAR Collaboration), PoS **CPOD2014**, 019 (2015).

[19] X. Luo, Nucl. Phys. A **956**, 75 (2016).

[20] X. Luo and N. Xu, Nucl. Sci. Tech. **28**, 112 (2017).

[21] J. Adam, L. Adamczyk, J. R. Adams, J. K. Adkins, G. Agakishiev, and M. M. Aggarwal, Phys. Rev. Lett. **126**, 092301 (2021).

[22] H. C. Song, S. A. Bass, U. Heinz, T. Hirano, and C. Shen, Phys. Rev. Lett. **106**, 192301 (2011).

[23] H. C. Song, S. A. Bass, and U. Heinz, Phys. Rev. C **83**, 024912 (2011).

[24] P. Deb, G. P. Kadam, and H. Mishra, Phys. Rev. D **94**, 094002 (2016).

[25] M. Leonhardt, M. Pospiech, B. Schallmo, J. Braun, C. Drischler, K. Hebeler, and A. Schwenk, Phys. Rev. Lett. **125**, 142502 (2020).

[26] F. G. Gardim, G. Giacalone, M. Luzum, and J. Y. Ollitrault, Nat. Phys. **16**, 615 (2020).

[27] D. Sahu, S. Tripathy, R. Sahoo, and A. R. Dash, Eur. Phys. J. A **56**, 187 (2020).

[28] D. Biswas, K. Deka, A. Jaiswal, and S. Roy, Phys. Rev. C **102**, 014912 (2020).

[29] A. Sorensen, D. Oliinychenko, V. Koch, and L. McLerran, Phys. Rev. Lett. **127**, 042303 (2021).

[30] K. T. Abe, Y. Tada, and I. Ueda, J. Cosmol. Astropart. Phys. **2021**, 048 (2021).

[31] B. Reed and C. J. Horowitz, Phys. Rev. C **101**, 045803 (2020).

[32] A. Kanakis-Pegios, P. S. Koliogiannis, and Ch. C. Moustakidis, Phys. Rev. C **102**, 055801 (2020).

[33] S. Han and M. Prakash, Astrophys. J. **899**, 164 (2020).

[34] I. Tews, J. Carlson, S. Gandolfi, and S. Reddy, Astrophys. J. **860**, 149 (2018).

[35] S. K. Greif, G. Raaijmakers, K. Hebeler, A. Schwenk, and A. L. Watts, Mon. Not. R. Astron. Soc. **485**, 5363 (2019).

[36] M. M. Forbes, S. Bose, S. Reddy, D. Zhou, A. Mukherjee, and S. De, Phys. Rev. D **100**, 083010 (2019).

[37] C. Drischler, S. Han, J. M. Lattimer, M. Prakash, S. Reddy, and T. Zhao, Phys. Rev. C **103**, 045808 (2021).

[38] R. Essick, I. Tews, P. Landry, S. Reddy, and D. E. Holz, Phys. Rev. C **102**, 055803 (2020).

[39] S. Han, M. A. A. Mamun, S. Lalit, C. Constantinou, and M. Prakash, Phys. Rev. D **100**, 103022 (2019).

[40] T. Kojo, AAPPS Bull. **31**, 11 (2021).

[41] S. Altiparmak, C. Ecker, and L. Rezzolla, Astrophys. J. Lett. **939**, L34 (2022).

[42] Ch. C. Moustakidis, T. Gaitanos, Ch. Margaritis, and G. A. Lalazissis, Phys. Rev. C **95**, 045801 (2017).

[43] N. Zhang, D. H. Wen, and H. Y. Chen, Phys. Rev. C **99**, 035803 (2019).

[44] Y. J. Huang, L. Baiotti, T. Kojo, K. Takami, H. Sotani, and H. Togashi, Phys. Rev. Lett. **129**, 181101 (2022).

[45] P. Jaikumar, A. Semposki, M. Prakash, and C. Constantinou, Phys. Rev. D **103**, 123009 (2021).

[46] O. Philipsen, Prog. Part. Nucl. Phys. **70**, 55 (2013).

[47] Y. Aoki, G. Endrodi, Z. Fodor, S. D. Katz, and K. K. Szabo, Nature (London) **443**, 675 (2006).

[48] S. Borsányi, Z. Fodor, C. Hoelbling, S. D. Katz, S. Krieg, and K. K. Sabzó, Phys. Lett. B **730**, 99 (2014).

[49] A. Bazavov, T. Bhattacharya, C. DeTar, H. T. Ding, S. Gottlieb, R. Gupta *et al.* (HotQCD Collaboration), Phys. Rev. D **90**, 094503 (2014).

[50] M. Motta, R. Stiele, W. M. Alberico, and A. Beraudo, Eur. Phys. J. C **80**, 770 (2020).

[51] S. K. Ghosh, T. K. Mukherjee, M. G. Mustafa, and R. Ray, Phys. Rev. D **73**, 114007 (2006).

[52] R. Marty, E. Bratkovskaya, W. Cassing, J. Aichelin, and H. Berrehrah, Phys. Rev. C **88**, 045204 (2013).

[53] K. Saha, S. Ghosh, S. Upadhaya, and S. Maity, Phys. Rev. D **97**, 116020 (2018).

[54] A. Abhishek, H. Mishra, and S. Ghosh, Phys. Rev. D **97**, 014005 (2018).

[55] R. Venugopalan and M. Prakash, Nucl. Phys. A **546**, 718 (1992).

[56] M. Bluhm, P. Alba, W. Alberico, A. Beraudo, and C. Ratti, Nucl. Phys. A **929**, 157 (2014).

[57] Z. V. Khaidukov, M. S. Lukashov, and Yu. A. Simonov, Phys. Rev. D **98**, 074031 (2018).

[58] Z. V. Khaidukov and Yu. A. Simonov, Phys. Rev. D **100**, 076009 (2019).

[59] V. Mykhaylova and C. Sasaki, Phys. Rev. D **103**, 014007 (2021).

[60] W. B. He, G. Y. Shao, X. Y. Gao, X. R. Yang, and C. L. Xie, Phys. Rev. D **105**, 094024 (2022).

[61] J. Pochodzalla, T. Mohlenkamp, T. Rubehn, A. Schuttauf, A. Worner, E. Zude *et al.* (ALADIN Collaboration), Phys. Rev. Lett. **75**, 1040 (1995).

[62] B. Borderie, G. Tabacaru, P. Chomaz, M. Colonna, A. Guarnera, M. Parlog *et al.* (NDRA Collaboration), Phys. Rev. Lett. **86**, 3252 (2001).

[63] A. S. Botvina, I. N. Mishustin, M. Begemann-Blaich, J. Hubele, G. Imme, I. Iori *et al.*, Nucl. Phys. A **584**, 737 (1995).

[64] M. D'Agostino, A. S. Botvina, l. M. Bruno, A. Bonasera, J. R. Bondorf, R. Bougault *et al.*, Nucl. Phys. A **650**, 329 (1999).

[65] B. K. Srivastava, R. P. Scharenberg, S. Albergo, F. Bieser, F. P. Brady, Z. Caccia *et al.* (EOS Collaboration), Phys. Rev. C **65**, 054617 (2002).

[66] J. B. Elliott *et al.* (ISiS Collaboration), Phys. Rev. Lett. **88**, 042701 (2002).

[67] P. Chomaz, M. Colonna, and J. Randrup, Phys. Rep. **389**, 263 (2004).

[68] Y. G. Ma, Phys. Rev. Lett. **83**, 3617 (1999).

[69] X. G. Deng, P. Danielewicz, Y. G. Ma, H. Lin, and Y. X. Zhang, Phys. Rev. C **105**, 064613 (2022).

[70] V. Vovchenko, M. I. Gorenstein, and H. Stoecker, Phys. Rev. Lett. **118**, 182301 (2017).

[71] G. Y. Shao, X. Y. Gao, and W. B. He, Phys. Rev. D **101**, 074029 (2020).

[72] N. K. Glendenning, *Compact Stars: Nuclear Physics, Particle Physics, and General Relativity* (Springer-Verlag, New York, 1997).

[73] M. Albright and J. I. Kapusta, Phys. Rev. C **93**, 014903 (2016).

[74] I. N. Mishustin, Phys. Rev. Lett. **82**, 4779 (1999).

[75] J. Randrup, Phys. Rev. Lett. **92**, 122301 (2004).

[76] V. Koch, A. Majumder, and J. Randrup, Phys. Rev. C **72**, 064903 (2005).

[77] C. Sasaki, B. Friman, and K. Redlich, Phys. Rev. Lett. **99**, 232301 (2007).

[78] C. Sasaki, B. Friman, and K. Redlich, Phys. Rev. D **77**, 034024 (2008).

[79] J. Randrup, Phys. Rev. C **79**, 054911 (2009); **82**, 034902 (2010).

[80] J. Steinheimer and J. Randrup, Phys. Rev. Lett. **109**, 212301 (2012).

[81] J. Steinheimer and J. Randrup, Eur. Phys. J. A **52**, 239 (2016).

[82] F. Li and C. M. Ko, Phys. Rev. C **93**, 035205 (2016).

[83] J. Steinheimer and V. Koch, Phys. Rev. C **96**, 034907 (2017).